buildings

MDPI

Article

Experimental Research on the Compression Property of Geopolymer Concrete with Molybdenum Tailings as a Building Material

Ming Sun [1], Yin Fu [2,*], Weixin Wang [2], Youzhi Yang [2] and An Wang [2]

[1] School of Traffic and Environment, Shenzhen Institute of Information Technology, Shenzhen 518172, China
[2] School of Civil Engineering, Tianjin University, Tianjin 300072, China
* Correspondence: fuyin_1996@tju.edu.cn

Abstract: This paper experimentally studied the effects of different molybdenum tailings (MoT) content, standard curing and 60 °C water curing conditions on the compressive strength of fly ash-based geopolymers at different ages. X-ray diffraction (XRD), scanning electron microscopy/energy dispersive spectrometer (SEM/EDS) and Fourier-transform infrared spectroscopy (FTIR) were applied to investigate the effect of the content of MoT and different curing conditions on the reaction products, microstructure and chemical composition of fly ash-based geopolymers. The results show that MoT content and curing conditions have synergistic effects on the compressive strength of fly ash-based geopolymers. For standard curing, the increase in MoT content is detrimental to the development of compressive strength, and an obvious weak interfacial transition zone between MoT and the gel product is observed in specimen containing 40 wt% MoT; meanwhile, under water curing conditions, the compressive strength of geopolymers first increases and then decreases with the increase in MoT, and the 28-day compressive strength can reach 90.3 MPa when the content of MoT is 10 wt%. The SEM results show that the curing conditions have a great influence on the microstructure of the geopolymer matrix, and the microstructure of the specimens under the water curing conditions is smoother and denser, with fewer pores. EDS analyses show that the gel product constituting the geopolymer matrix is N(C)-A-S-H gel; MoT can participate in the reaction, and the mass ratio of Ca/(Si + Al) of N(C)-A-S-H gel increases with the increase in MoT, resulting in a decrease in compressive strength. In addition, the results of the FTIR confirm that water curing can increase the degree of crosslinks in the gel phase.

Keywords: geopolymer; molybdenum tailings; compressive strength; curing condition; microstructure

Citation: Sun, M.; Fu, Y.; Wang, W.; Yang, Y.; Wang, A. Experimental Research on the Compression Property of Geopolymer Concrete with Molybdenum Tailings as a Building Material. *Buildings* **2022**, *12*, 1596. https://doi.org/10.3390/buildings12101596

Academic Editor: Jan Fořt

Received: 5 September 2022
Accepted: 29 September 2022
Published: 3 October 2022

1. Introduction

Molybdenum tailings (MoT) are solid wastes produced during the beneficiation of molybdenum ore. Due to the low utilization rate of molybdenum ore, the output of MoT is huge, and 36 million tons of molybdenum tailings are discarded in China every year [1]. At the same time, with the widespread use of molybdenum in various industries [2], the rate with which it is mined is increasing rapidly, and the stock of MoT is bound to increase. Like other tailings, the storage of MoT does not only occupy a large area of land, but also causes secondary disasters under extreme weather, such as dam failure and endangerment of the living environment. In addition, the toxic elements in MoT may penetrate into the soil, causing environmental pollution [3]. Therefore, how to realize the reduction and reuse of MoT has attracted extensive attention worldwide.

Due to the nonrenewable nature of natural river sand used in the construction industry, it has gradually become a hot topic of research to find a recycled aggregate material to replace natural river sand. The chemical composition and physical properties of MoT are similar to those of natural river sand. Therefore, much of the literature has explored the feasibility of MoT to replace river sand as fine aggregate in cement-based materials [4].

Quan et al. [4] reported that the compressive strength of concrete prepared by using MoT to replace natural river sand decreased with the increase in MoT substitution rate. Gao et al. [5] reported that, when the ratio of MoT to replace natural sand is high, the use of MoT in CFST columns is a better solution, and the compressive strength of the sample with a 100% MoT replacement rate is only reduced by about 10%. Quan et al. [6] used MoT to prepare recycled aggregate concrete, and the 28-day compressive strength of recycled aggregate concrete with a replacement rate of 50% MoT exceeded 45 MPa. However, cement-based materials have the disadvantages of high energy consumption and high carbon dioxide emissions, and the use of cement-based materials to dispose of MoT undoubtedly has certain negative impacts on the environment. Geopolymers are used as a gel material to replace cement because of their lower carbon footprint and excellent performance similar to cement-based materials [7], becoming a new strategy for reduction and reuse of MoT [8]. Due to its low reactivity, the MoT used for geopolymer preparation need to be pretreated to improve their activity in an alkaline medium. Li et al. [9] reported that the mechanical alkali melting activation method can effectively improve the activity of MoT, and the alkaline leaching of both Si and Al of MoT can reach above 1500 mg/L. Li et al. [10] used activated MoT as the raw material and modified sodium silicate solution as the alkaline activator for geopolymer synthesis and reported that, with the modulus of modified sodium silicate solution being 1.6, the Si/Al molar ratio being 2.8 and the liquid-to-solid mass ratio being 3.0, the compressive strength reached 51.3 MPa under standard curing for 28 days. Moreover, research on the preparation of geopolymers using MoT without any pretreatment and additional aluminosilicate sources are reported by some researchers. Han et al. [11] applied acoustic emission technology to investigate the effect of MoT on the fracture behavior of fly ash-based geopolymers, and reported that the addition of 20 wt% MoT can significantly improve the flexural strength and early fracture toughness of geopolymers; however, the literature lacks the analysis of macroscopic performance by means of different microscopic characterization methods. Wang et al. [12] used 80 wt% garnet tailings from molybdenum ore and 20 wt% metakaolin to prepare a geopolymer with a 3-day compressive strength of 45 MPa, but the metakaolin used needs to be calcined at high temperature to be active, so this pretreatment causes a certain amount of energy consumption. Without further calcination pretreatment, fly ash (FA) is a common artificial aluminosilicate raw material for synthesizing geopolymers [13]. Since the chemical composition of MoT is similar to that of aluminosilicates, they have a degree of chemical reactivity and make it possible to prepare geopolymers as aluminosilicate raw materials [9]. Moreover, there are many studies concerning geopolymers using only one type of curing condition [14,15], limiting the application of geopolymers in more curing conditions. Therefore, in order to broaden the application range of fly ash-based geopolymer concrete with MoT, the compression property and influencing factors of using FA and MoT as raw materials to prepare geopolymers subjected to different curing conditions need to be studied. In addition, the relationship between the compression property and curing conditions of geopolymers prepared from MoT and FA is still unclear.

In this paper, FA and MoT are used as aluminosilicate raw materials to prepare geopolymers. The effects of MoT content and curing conditions on its compressive strength properties were studied. Finally, combined with X-ray diffraction (XRD), scanning electron microscopy and energy dispersive analysis (SEM/EDS) and Fourier-transform infrared spectroscopy (FTIR), the effect of the reaction products, microscopic morphology and chemical composition on the compression property was analyzed.

2. Materials and Methods

2.1. Materials

The raw materials used for geopolymer preparation are MoT and FA. The MoT were provided by Luanchuan County, Henan Province, and the FA was supplied by a thermal power plant in Qinhuangdao, Hebei Province, China. Table 1 shows the chemical composition of the MoT and FA used in this study. It can be seen that the MoT are composed of

SiO_2, CaO and Fe_2O_3, while the fly ash mainly contains SiO_2 and Al_2O_3. Figure 1 shows the microstructures of MoT and FA, where MoT are composed of particles with irregular edges, while fly ash is mainly composed of spherical particles.

Table 1. Chemical composition of molybdenum tailings and fly ash (wt%).

Chemical Composition	MoT	FA
SiO_2	41.842	38.0
Al_2O_3	5.801	37.7
CaO	29.9	6.35
Fe_2O_3	15.172	4.97
Na_2O	-	0.902
MgO	2.057	0.873
K_2O	0.822	1.06
SO_3	2.363	0.970
MoO_3	0.021	-
TiO_2	0.389	1.67
P_2O_5	0.175	0.457
WO_3	0.049	-
ZnO	0.029	0.0289
Cr_2O_3	0.026	0.0153
ZrO_2	0.02	0.101
V_2O_5	0.009	0.0332
SrO	0.007	0.236
Y_2O_3	0.002	0.0110
LOI	1.316	6.6226

Note: LOI = loss on ignition at 1000 °C.

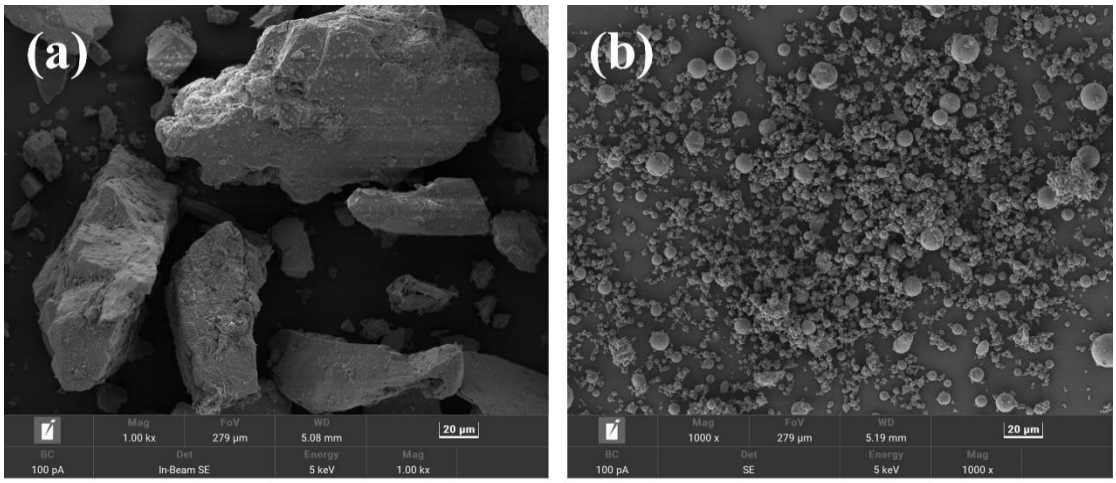

Figure 1. Micromorphology of MoT (**a**) and FA (**b**).

Figure 2 presents the XRD patterns of MoT and FA. MoT have high crystallinity, mainly including the crystalline phases of quartz (SiO_2, PDF#79-1906), andradite ($Ca_3Fe_2Si_3O_{12}$, PDF#76-0874), calcite ($CaCO_3$, PDF#88-1809), sanidine high ($K(AlSi_3O_8)$), PDF#80-2109) and anorthite ($Ca(Al_2Si_2O_8$, PDF#86-1707). It can be seen from Figure 3b that, within the range of 2θ from 10 degrees to 40 degrees, the XRD pattern of FA has a hump diffraction peak associated with the amorphous phase. In addition, fly ash also contains certain crystalline phases such as mullite, syn ($Al_2(Al_{2.8}Si_{1.2})$ $O_{9.6}$, PDF#79-1275), corundum (Al_2O_3, PDF#74-1081) and quartz low (SiO_2), PDF#85-0335). According to the micromorphology and XRD analysis of MoT, the MoT used in this study have a large particle size and high crystallinity, which indicates their low reactivity.

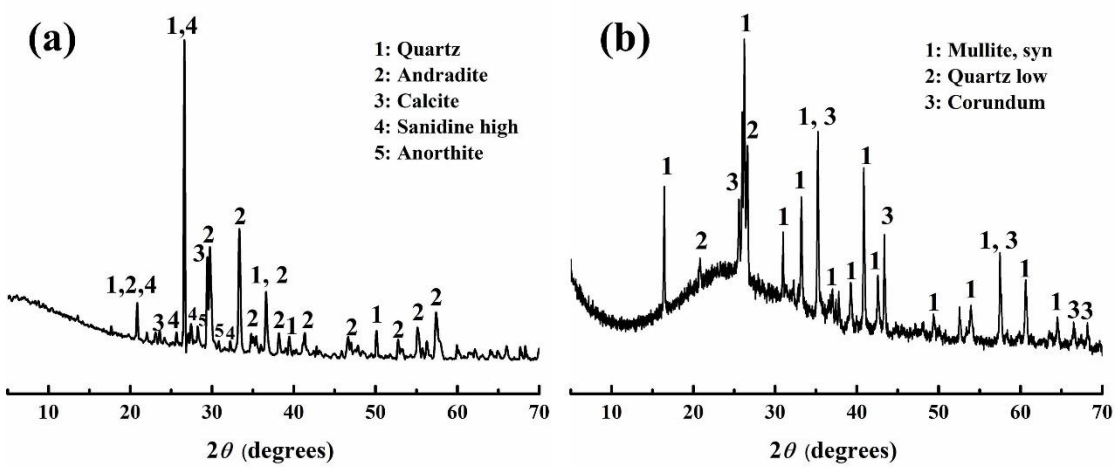

Figure 2. XRD patterns of MoT (**a**) and FA (**b**).

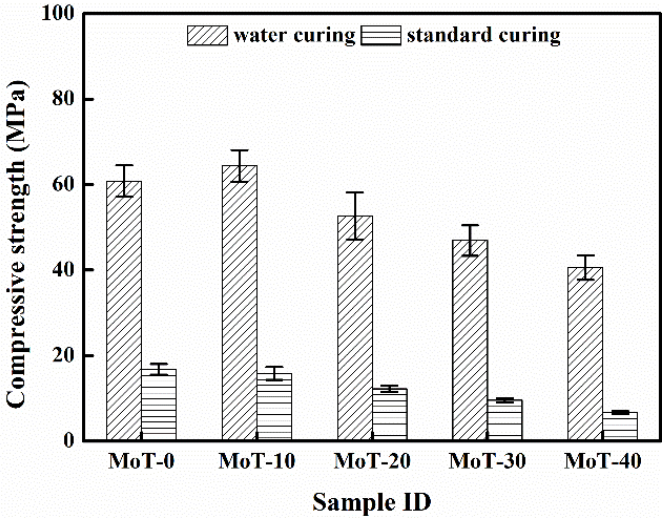

(**a**) 3 d

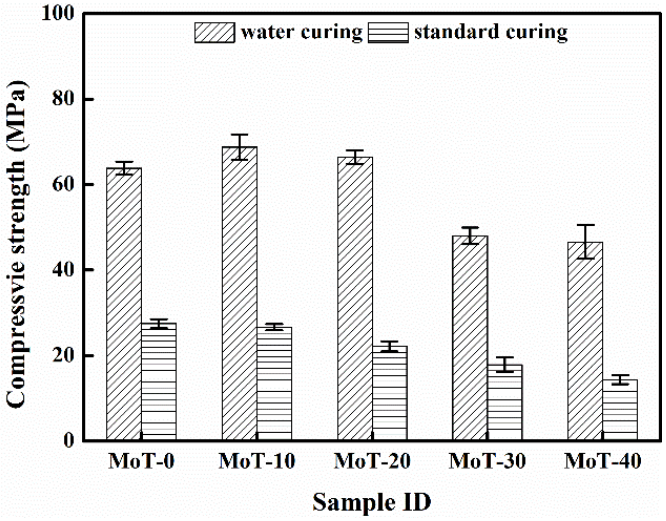

(**b**) 7 d

Figure 3. *Cont*.

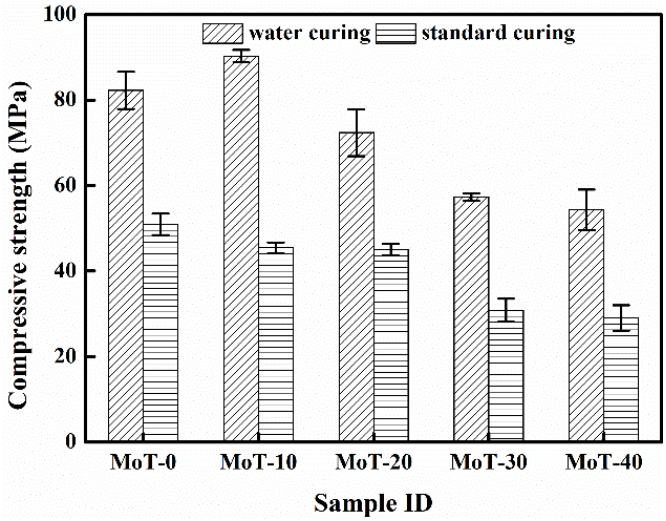

(**c**) 28 d

Figure 3. Effects of MoT content and curing condition on the compressive strength of the specimens.

Sodium silicate solution and solid sodium hydroxide particles were used to prepare the alkaline activated solution (AAS). Sodium silicate solution (8.2% SiO_2, 26% SiO_2 and 65.7% H_2O, modulus 3.1) was purchased from Zhongfa Water Glass Factory in Guangdong Province. Solid sodium hydroxide particles (96% purity) were produced by Shanghai Merrill Technology Company. The solid sodium hydroxide particles were added to the sodium silicate solution, and the modulus of the sodium silicate solution was adjusted to 1.5 to obtain the AAS required for the test. Under this modulus, the AAS can provide a good alkaline environment and sufficient active silica for the reaction, and fly ash-based geopolymers with excellent properties can be obtained [16].

2.2. Mix Design and Sample Preparation

Table 2 lists the five groups of mix proportions used in this study. According to the MoT content that is the mass ratio of MoT to raw materials (MoT + FA), five groups of mix proportions are designed. The designed mass ratios of five groups of mix proportions are 0 wt%, 10 wt%, 20 wt%, 30 wt% and 40 wt%, and the samples corresponding to these five groups are denoted as MoT-0, MoT-10, MoT-20, MoT-30 and MoT-40, respectively. For all mix proportions, the mass ratio of AAS to raw material was 0.3.

Table 2. Mix proportion of investigated geopolymer.

Sample ID	Raw Materials		AAS/Raw Materials Mass Ratio
	MoT (wt%)	FA (wt%)	
MoT-0	0	100	0.3
MoT-10	10	90	
MoT-20	20	80	
MoT-30	30	70	
MoT-40	40	60	

Due to the exothermicity of sodium hydroxide in water, the AAS should be prepared one day in advance and cooled to room temperature for later use. The sample preparation process was illustrated as follows. First, the raw materials were poured into the mixer and stirred for 2 min to mix the raw materials evenly; then, the AAS was slowly poured into the raw materials and the mixture was stirred for another 2 min to make the slurry uniform; the obtained slurry was then poured into molds with a size of 40 mm × 40 mm × 40 mm, and a vibrating table was used to vibrate the specimens for 1 min to discharge the air bubbles

introduced into the slurry during the stirring process; finally, the surface of the specimens was covered with a piece of PE film to prevent water loss; all specimens were cured at room temperature for 1 day and then demolded. After demoulding, the five groups of specimens were cured in two ways: (1) standard curing (25 °C, humidity > 95%); (2) water curing (60 °C). The curing age was set to 3, 7 and 28 days. In this study, the compressive strength test of the specimens was carried out on days 3, 7 and 28 of curing.

2.3. Instrumentation and Measurements

2.3.1. Compressive Strength Test

The compressive strength tests were conducted on each group of specimens cured to corresponding ages under the two curing mechanisms. For each group of specimens, six specimens were taken for compressive strength testing at each curing age. The compressive strength of the specimens was measured using a multifunctional compressive testing machine (YAW-300C, Jinan Shidaishijin Testing Machine Co., Ltd., Jinan, China) at a loading rate of 2.4 kN/s, according to the GB/T 17671-2021 standard. In order to obtain reliable test results, the average value of the six obtained test data is taken as the compressive strength of the proportioning sample at this age.

2.3.2. XRD

In order to determine the differences in the mineral composition of geopolymers with different curing ages and curing mechanisms, the mineral compositions of the samples under different curing mechanisms were analyzed by XRD. The small pieces of the core of the sample were collected after the compressive strength test, and these small pieces were vacuumed in a vacuum drying oven and then ground into powders smaller than 0.074 μm. These powers were the samples for XRD testing. The samples were analyzed by using a Bruker Advance D8 X-ray diffractometer (Bruker Corporation, Germany). The samples were scanned in a range of 5°to 70° (2θ), with an increment of 10° (2θ) every 1 min.

2.3.3. SEM/EDS

In this study, scanning electron microscopy was used to observe the microscopic morphology of the geopolymer, and EDS was used to analyze its elemental composition. A flake-like block smaller than 1 cm^2 was collected from the core of the specimen after compressive strength testing as a sample for SEM testing. The sample was directly adhered to the conductive adhesive and sprayed with gold for 60 s using an Oxford Quorum SC7620 sputtering coater, and the gold spray was 10 mA; then, the scanning electron microscope (TESCAN MIRA LMS, Czech Republic) was used to photograph the sample morphology and energy spectrum mapping test, and the morphology was photographed. The acceleration voltage was 3 kV, the acceleration voltage was 15 kV during energy spectrum mapping and the detector was an SE2 secondary electron detector.

2.3.4. FTIR

Infrared spectra of finely ground hardened powder samples were recorded by a Fourier infrared spectrometer Nicolet iS20 (Thermo Scientific, Waltham, MA, USA). For the analysis, 1 to 2 mg of the powder sample and 200 mg pure KBr were fully ground many times to make it even in a dry environment, then pressed into a transparent sheet on a hydraulic press; then, the sample was placed into the infrared spectrometer for testing. The wave number range is 4000 to 400 cm^{-1}; 32 scans per sample were made, with a resolution of 4 cm^{-1}.

3. Results and Discussion

3.1. Compressive Strength

Figure 3 shows the effect of MoT content and curing condition on the compressive strength of geopolymer specimens. It can be observed that the compressive strength of the water curing specimen was significantly higher than the corresponding standard

curing specimen. Compared with the standard curing condition, the increase of curing temperature for water curing accelerated the migration of Na^+ and OH^- in the matrix, which promoted the process of the release of active silicon and aluminum by alkali erosion of amorphous soluble aluminosilicate in fly ash, thereby promoting the hydration process of the amorphous aluminosilicate gel. These gel products are generally considered to be the main source of the strength of the fly ash geopolymer matrix [17]. Furthermore, as reported in Equation (1) in [18], the process of reactive aluminosilicates releasing free SiO^{4-} and AlO^{4-} tetrahedral units in a highly alkaline environment required water. Due to the osmotic effect of water, compared with the standard curing mechanism, the water curing mechanism can indirectly provide more water for the reaction under the same alkaline conditions, thereby providing favorable conditions for the subsequent geopolymer condensation reaction.

$$(Si_2O_5, Al_2O_2)_n + nH_2O \xrightarrow{NaOH} n(OH)_3 - Si - O - Al - (OH)_3 \quad (1)$$

The compressive strength of the geopolymer decreased with the increase in MoT content under standard curing conditions; for example, the compressive strength of MoT-40 at 3 d, 7 d and 28 d decreased by 60.1%, 47.6% and 43.0% compared with that of MoT-0, respectively. On the one hand, this is because the increase in MoT led to a relative decrease in the content of fly ash, whose soluble aluminosilicate components can be dissolved in an alkaline medium, thereby reducing the active components in the raw material and further reducing the gel amount of product. On the other hand, since MoT contained 15.172 wt% Fe_2O_3, their presence may inhibit the progress of the alkaline-activated reaction and the formation of the gel phase [19]. In addition, since the microscopic morphology of MoT is relatively smooth, the interfacial bond between it and the gel product is weak. Therefore, the quality of the interfacial bond between the gel product and MoT as aggregate deteriorates with the increase in MoT, which can be confirmed by SEM analysis. For the water curing mechanism, the trend of compressive strength of the geopolymer showed that it first increased and then decreased with the addition of MoT, and the maximum compressive strength value at each age appeared in MoT-10, which was 64.4 MPa for 3 days, 68.7 MPa for 7 days and 90.3 MPa for 28 days. The excellent compressive properties of MoT-10 can be attributed to the following three reasons. First, due to its large particle size and low activity, MoT can play the role of aggregate in the geopolymer matrix, and the MoT with a irregular shape, acting as the aggregate, can be tightly bound with the surrounding gel product, reducing the micro-stress during the failure process [20]. Secondly, under this curing condition and MoT content, both MoT and fly ash may react with the AAS, and their synergistic effect makes the microstructure of the geopolymer more compact, thereby improving the compressive strength. Finally, similar to the strength degradation mechanism of compressive strength with MoT content under the standard curing mechanism mentioned above, the continuous addition of MoT led to a decrease in the quality and quantity of the gel product, and finally caused a decrease in the compressive strength. The above test results show that the content of MoT and the curing mechanism have a synergistic effect on the development of the compressive strength of fly ash-based geopolymers.

3.2. XRD Analysis

XRD analysis was used to study the effect of MoT content and curing mechanism on the phase change of geopolymers. The XRD patterns of the samples cured for 28 days under standard curing (a) and water curing (b) are shown in Figure 4. Due to the dilution effect, the diffraction peak intensity in the geopolymer sample with the addition of MoT was weaker than that of the raw material [8], but obvious diffraction peaks were still detected in the two patterns, and their corresponding phases were mullite, corundum, quartz, andradite and calcite. Among them, quartz was derived from FA and MoT, andradite and calcite came from MoT and corundum came mainly from FA. SEM analysis confirmed that there were residual MoT and FA particles in the sample. It can also be seen that

with the increase in the content of MoT, orthoclase (PDF#71-1540, KSi_3AlO_8) appeared in the standard curing MoT-30 and orthoclase and albite low (PDF#74-0603, $Na(Si_3AlO_8)$) appeared in the standard curing MoT-40, which may be due to the phase transformation in MoT. As for water bath curing, rankinite (PDF#76-0623, $Ca_3Si_2O_7$) and kyanite (PDF#72-1447, Al_2SiO_6) appeared in MoT-20 and MoT-30, respectively, which may be ascribed to the high curing temperature and humidity. For the two curing mechanisms, the diffraction peak intensities of quartz and andradite were enhanced with the increase in the content of MoT, and the quartz phase was not easily eroded by alkali [21], resulting in a relative reduction in the soluble silica provided for the reaction, which in turn caused a relative reduction in the gel product that provides strength to the geopolymer [22], thus causing a decrease in compressive strength with excessive addition of MoT.

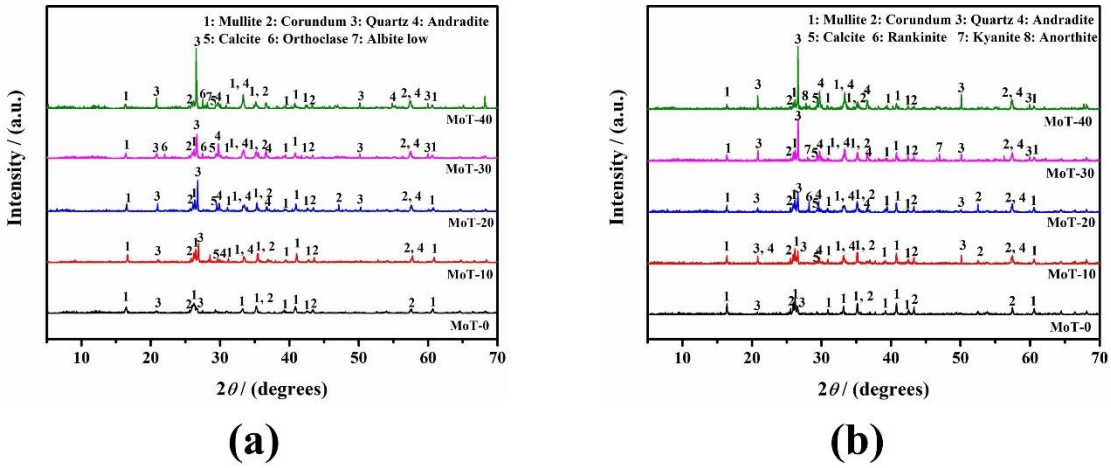

Figure 4. XRD patterns of samples cured for 28 days: (**a**) standard curing; (**b**) water curing.

3.3. SEM/EDS Analysis

Figures 5 and 6 show the microscopic morphology and EDS analyses of MoT-0 and MoT-40 at 28 days of standard curing, respectively; Figures 5f and 6f are the EDS results of Area 1 and Area 2, respectively. Under standard curing conditions, the main microscopic morphologies of MoT-0 include gel products, concave pits, unreacted fly ash particles, partially reacted fly ash particles, voids and cracks. There were two reasons for the formation of the concave pits. First, the original spherical fly ash particle at this position was completely dissolved by alkali; second, some unreacted fly ash particles are not combined tightly with the geopolymer gel matrix during the destruction process and peeled off. The shrinkage generated during the curing process of the specimen causes cracks around the vitreous body of fly ash [23]. With the addition of MoT, the microscopic morphology of the specimen became uneven. At the same time, it can be observed that there were MoT partially embedded in the gel phase (Figure 6c), and this part of the MoT acted as an aggregate and was closely combined with the surrounding geopolymer matrix; however, since the surface of the MoT was relatively smooth, some MoT may not effectively bond with the gel, thus creating a weak interfacial transition zone (ITZ) between the MoT and the gel matrix (Figure 6d), which was undoubtedly detrimental to strength development. From the EDS analyses of Areas 1 and 2, the addition of MoT also affected the microscopic elemental composition of the gel phase. The Ca/(Si + Al) mass ratio of MoT-40 was much larger than that of MoT-0, which indicated that the active Si and Al in the FA of MoT-40 were not fully activated by alkali, and the degree of participation in the reaction was low, which adversely influenced the compressive strength [24]. Meanwhile, EDS analysis confirmed that the gel phase was mainly amorphous N(C)-A-S-H gel, a common gel product of fly ash-based geopolymers [25]. It is worth noting that the element composition of the gel

phase of MoT-40 also included Mo, which showed that MoT can be dissolved under this condition to release Mo and participate in the formation of gel products.

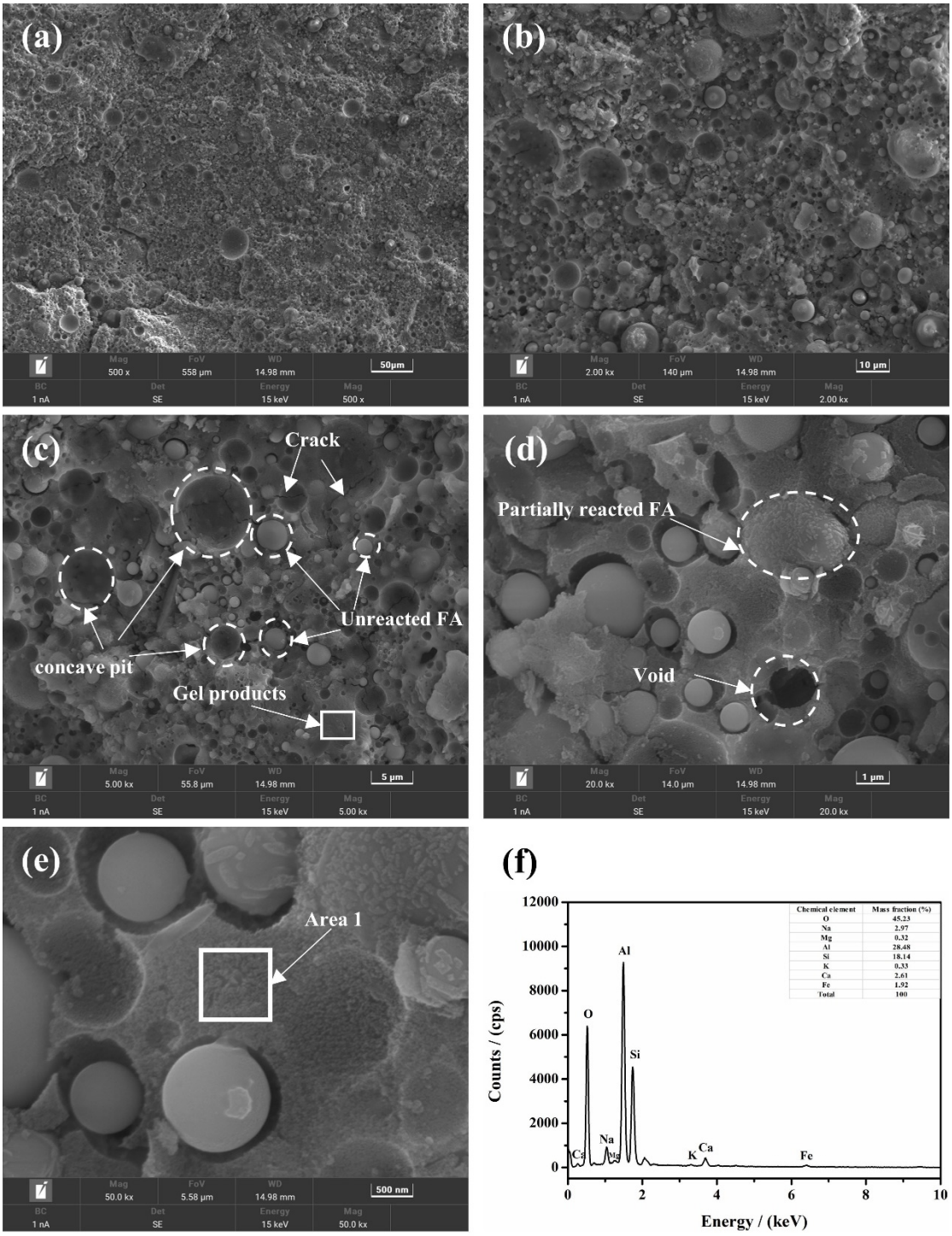

Figure 5. Microstructure of MoT-0 at 28 days of standard curing: (**a**) 500 ×; (**b**) 2 k×; (**c**) 5 k×; (**d**) 20 k×; (**e**) 50 k×; (**f**) EDS of Area 1.

Figures 7–9 show the microscopic morphology and EDS analyses of MoT-0, MoT-10 and MoT-40 cured for 28 days under water curing, respectively. With the increase in MoT content, the microstructure of the sample became loose and porous. From the EDS analysis results of Areas 3 and 4, it can be seen that the mass ratio of Ca/(Si + Al) in the gel phase

increases with the increase in MoT content, which is consistent with the results of standard curing conditions. Moreover, no exposed MoT particles were observed on the surface of MoT-10 and MoT-40, which indicated that the MoT particles were physically well bound and encapsulated by the gel product N(C)-A-S-H. Compared with the standard curing specimens, the microstructure of the specimens under water curing was more compact, and the microstructure had fewer fly ash particles on the surface, fewer cracks and voids, and a denser gel matrix, which was well reflected in compressive strength results.

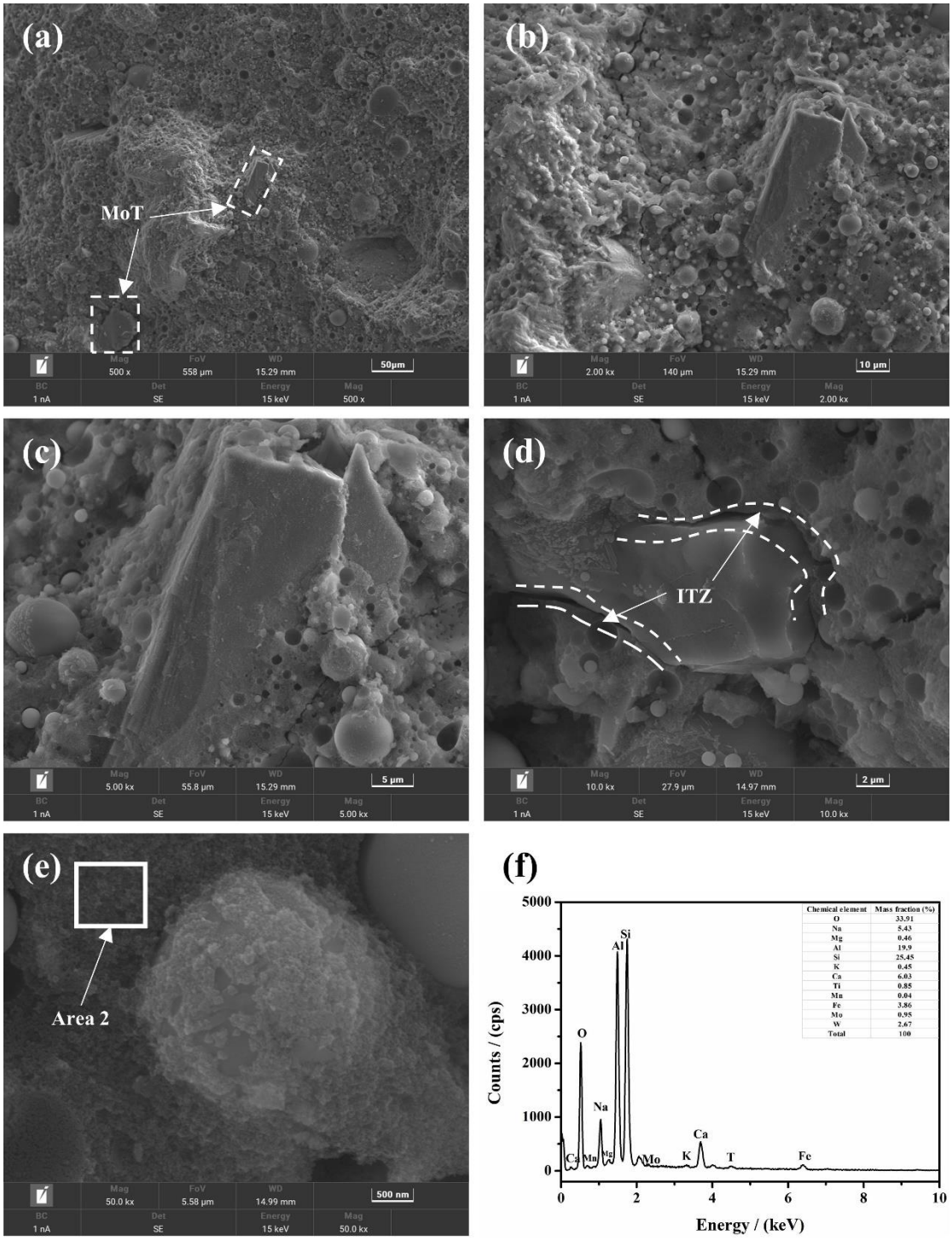

Figure 6. Microstructure of MoT-40 at 28 days of standard curing: (**a**) 500 ×; (**b**) 2 k×; (**c**) 5 k×; (**d**) 10 k×; (**e**) 50 k×; (**f**) EDS of Area 2.

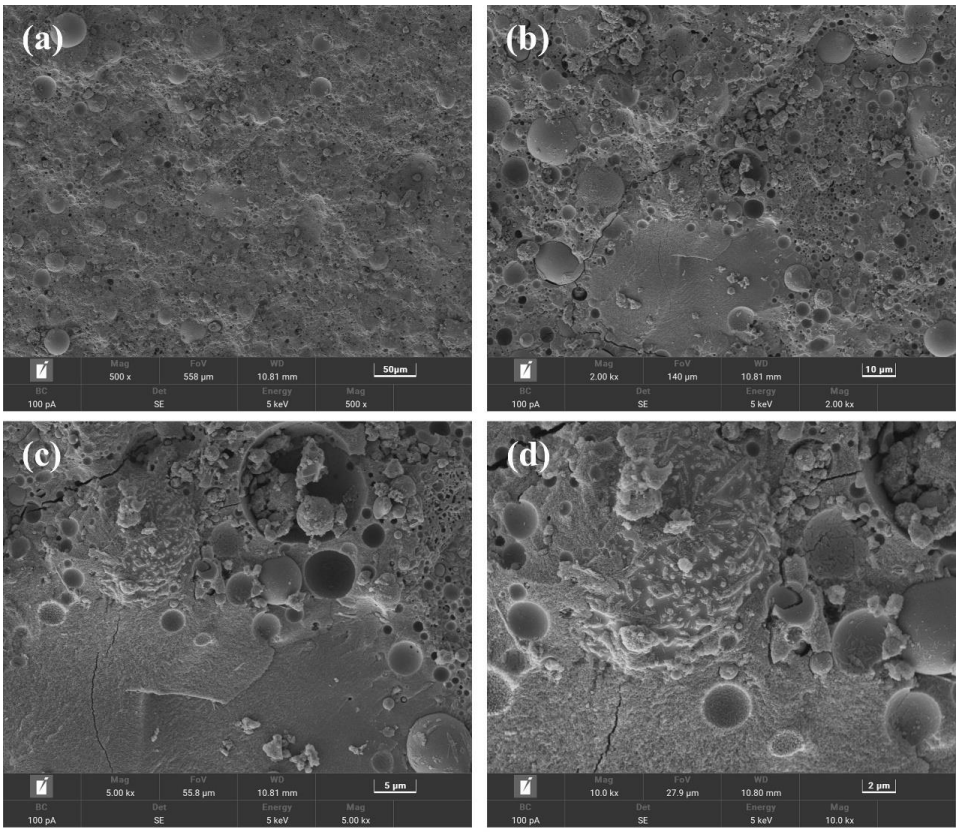

Figure 7. Microstructure of MoT-0 at 28 days of water curing: (**a**) 500 ×; (**b**) 2 k×; (**c**) 5 k×; (**d**) 10 k×.

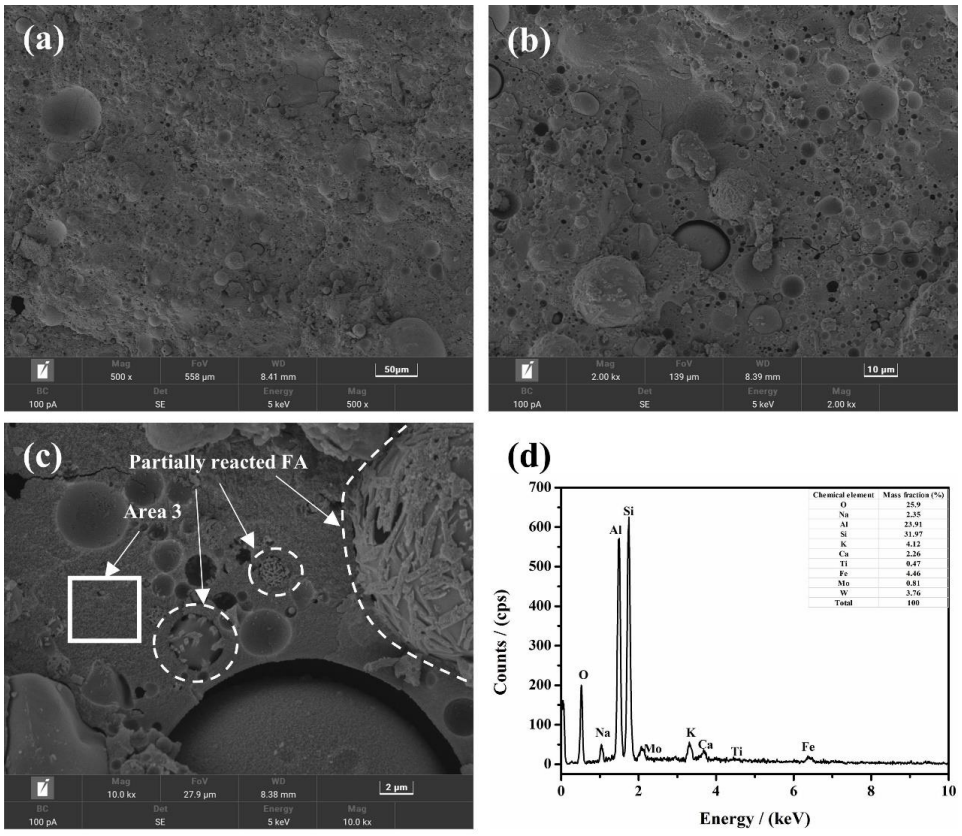

Figure 8. Microstructure of MoT-10 at 28 days of water curing: (**a**) 500 ×; (**b**) 2 k×; (**c**)10 k×; (**d**) EDS of Area 3.

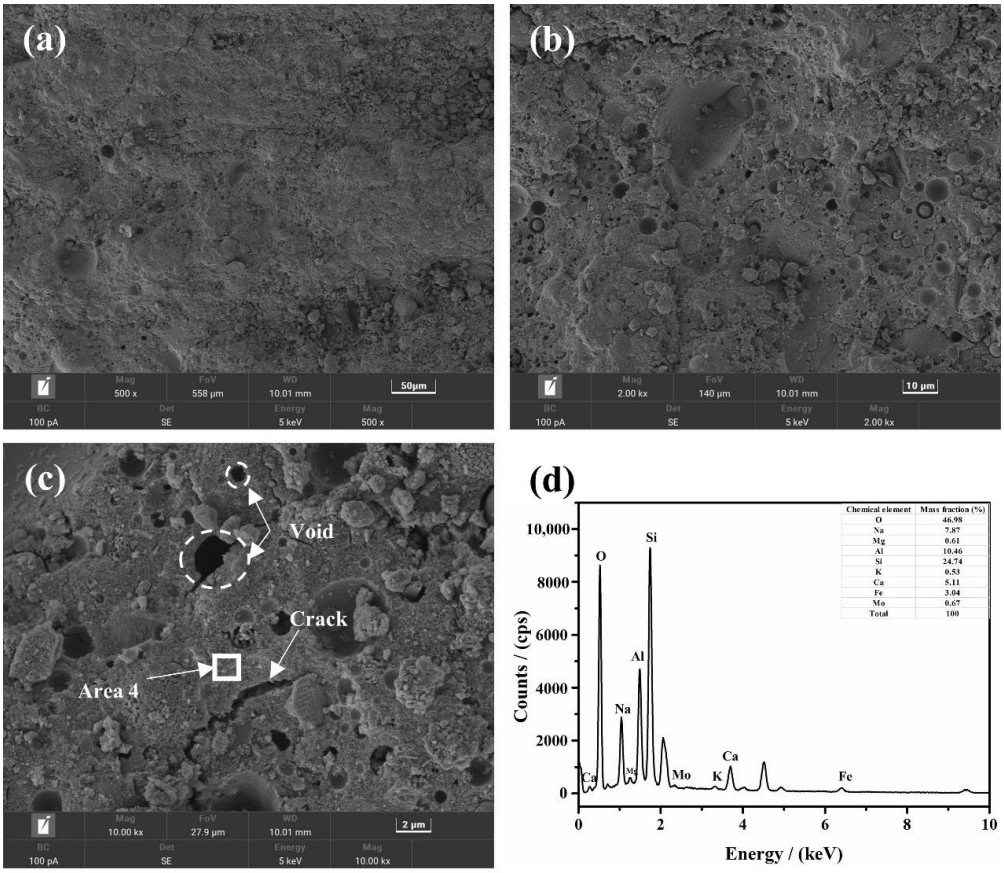

Figure 9. Microstructure of MoT-40 at 28 days of water curing: (**a**) 500 ×; (**b**) 2 k×; (**c**) 10 k×; (**d**) EDS of Area 4.

3.4. FTIR Analysis

Figure 10a,b show the FTIR spectra of standard-cured and water bath-cured samples at 28 days, respectively. The absorption bands appearing in the wavenumber range from about 3424 to 3445 cm^{-1} represent the stretching vibration of O-H, and the absorption band appearing around 1645 cm^{-1} shows the presence of bending vibration of O-H in the chemically bound water of the gel phase [26]. The peak located at 1429 to 1471 cm^{-1} correlates with the O-C-O stretching vibration of the carbonate phase, which may originate from the reaction of the alkali activator and carbon dioxide [27] and carbonate phase in MoT, such as calcite. The intensity of this peak became stronger with the increase in MoT, indicating that the degree of carbonization of the sample increased. Compared with the standard curing condition, the intensity of this peak was weaker under the water curing condition; this was because the water around the specimens isolated the specimen from the contact of air, and it was not easy to keep the carbon dioxide in the water at 60 °C, which was beneficial to prevent the carbonization of the sample. The absorption peak observed around the wavenumber of 1010 cm^{-1} represented the asymmetric stretching vibration of the Si-O-Si(Al) in the gel product N(C)-A-S-H [28]. Compared with the standard curing, the characteristic peaks corresponding to Si-O-Si (Al) of the specimens under the water curing conditions shifted to lower wavenumbers. This illustrated that some of the $[SiO4]^{4-}$ in the tetrahedral Si–O–Si(Al) network structure in the geopolymer gel were replaced by $[AlO4]^{5-}$, which indicated that the water curing can promote more Al to be introduced in the geopolymer gel and increases the crosslinking degree of the gel phase [13], leading to a denser microstructure of the samples subjected to water curing. Therefore, under the same MoT content, the compressive strength of samples under water curing was higher than that under standard curing. The absorption band representing the stretching vibration of Si-O-Si in quartz appeared at 730 cm^{-1}; its peak intensity was obvious only in MoT-0 and

MoT-10 under water curing [27]. The band with a wavenumber of 560 cm^{-1} appearing in MoT-0 and MoT-10 represents the stretching vibration of Al-O [29]; this peak belonged to the [AlO_6] structure in the mullite phase and decreased with the increase in MoT content. The peak around 460 cm^{-1} represented the bending vibration of Si-O [30].

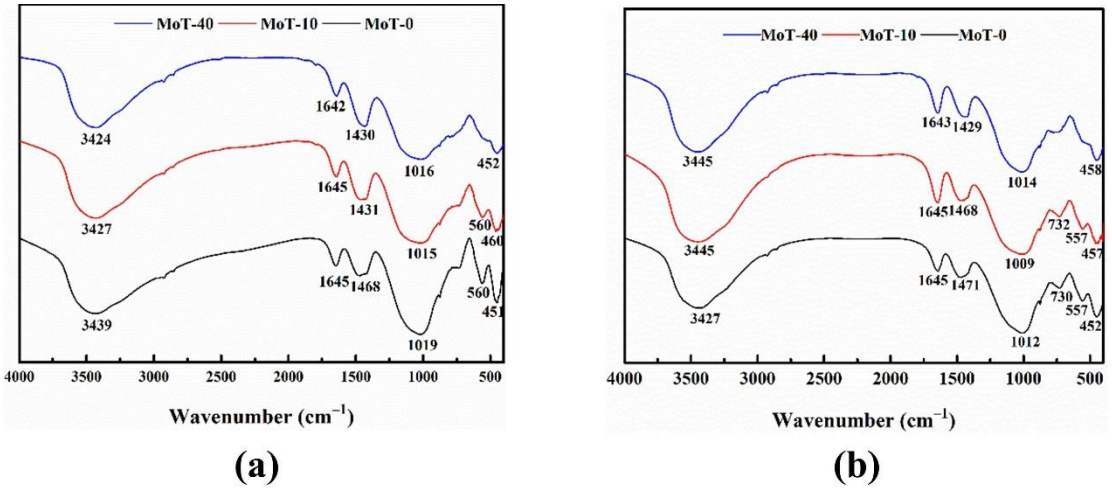

Figure 10. FTIR spectra of samples at 28 days: (**a**) standard curing; (**b**) water curing.

4. Conclusions

The scientific objectives of this work were to investigate the effect of different MoT contents and curing conditions on the compression property of fly ash-based geopolymers modified by MoT. Based on the experimental results and analyses obtained in this study, conclusions can be drawn as follows:

(1) The compression property of fly ash-based geopolymers is related to the MoT content. With the increase in MoT substitution rate, the compressive strength of fly ash-based geopolymers showed a decreasing trend under standard curing conditions, while the compressive strength of geopolymers under water curing conditions first increased and then decreased. When the substitution rate of MoT to FA was 10%, the compressive strength of the geopolymer cured in a water bath for 28 days was 90.3 MPa.

(2) MoT can participate in the reaction and change the microstructure and chemical composition of fly ash-based geopolymers. With the increase in the proportion of MoT instead of FA, the mass ratio of Ca/(Si + Al) in the reaction product increases, which affects the development of the mechanical properties of the geopolymer. At the same time, the excessive addition of MoT makes the microstructure of the geopolymer matrix uneven, causing a weak interfacial transition zone between MoT and the gel, resulting in a decrease in strength.

(3) The curing conditions affect the compression property of the fly ash-based geopolymer. The compression property of fly ash-based geopolymers under water curing are better than those under standard curing. Meanwhile, water curing also contributed to the early and final strength development of fly ash-based geopolymers, and this trend was related to the microscopic morphology of gel products and the degree of crosslinking of the gel products. The SEM results show that the microscopic morphology of the specimens under water curing was more compact, and the FTIR results show that water curing can promote more Al to enter the geopolymer gel and improve the crosslinking degree of the gel phase.

(4) MoT substitution rate and curing conditions have synergistic effects on the compression property of fly ash-based geopolymers. The degree of deterioration of the compressive strength of the standard curing specimens has a large correlation with the MoT substitution rate, but the degree to which the compressive strength of the

specimens cured in the water bath decreased has little correlation with the increase in the MoT content.

(5) The application of MoT to fly ash-based geopolymers in this study has provided an effective experience and confidence for further utilization of this material as a prefabricated material. However, more mechanical properties of MoT–fly ash-based geopolymers, such as compressive stress-strain curves, flexural strength and anti-splitting ability, still need further research. In addition, its further structural application in larger components will be systematically explored in the future.

Author Contributions: Conceptualization, M.S. and Y.F.; methodology, M.S. and Y.F.; resources, writing—original draft preparation, Y.F.; review and editing, W.W., A.W. and Y.Y.; funding acquisition, M.S.; All authors have read and agreed to the published version of the manuscript.

Funding: This work was financially supported by Shenzhen High-level Talents Research Start-up Fund (11400-2022-010201-12) and Shenzhen Institute of Information Technology Research Start-up Fund (Grant No. SZIIT2022KJ015).

Data Availability Statement: Data sharing is not applicable.

Conflicts of Interest: The authors declare no conflict of interest.

References

1. Gao, S.; Cui, X.W.; Zhang, S.M. Utilization of Molybdenum Tailings in Concrete Manufacturing: A Review. *Appl. Sci.* **2020**, *10*, 138. [CrossRef]
2. Shmelev, A.N.; Kozhahmet, B.K. Use of molybdenum as a structural material of fuel elements for improving the safety of nuclear reactors. In Proceedings of the International Conference on Young Scientists, Specialists, and Postgraduates on Nuclear Reactor Physics (ICNRP), Moscow, Russia, 5–9 September 2016.
3. Zhang, W.; Long, J.H.; Zhang, X.R.; Shen, W.N.; Wei, Z.Y. Pollution and Ecological Risk Evaluation of Heavy Metals in the Soil and Sediment around the HTM Tailings Pond, Northeastern China. *Int. J. Environ. Res. Public Health* **2020**, *17*, 7072. [CrossRef] [PubMed]
4. Quan, X.Y.; Wang, S.L.; Liu, K.N.; Xu, J.; Zhao, N.; Liu, B. Evaluation of molybdenum tailings as replacement for fine aggregate in concrete: Mechanical, corrosion resistance, and pore microstructural characteristics. *Constr. Build. Mater.* **2022**, *343*, 127982. [CrossRef]
5. Gao, S.; Cui, X.; Kang, S.; Ding, Y. Sustainable applications for utilizing molybdenum tailings in concrete. *J. Clean. Prod.* **2020**, *266*, 122020. [CrossRef]
6. Quan, X.; Wang, S.; Li, J.; Luo, J.; Liu, K.; Xu, J.; Zhao, N.; Liu, Y. Utilization of molybdenum tailings as fine aggregate in recycled aggregate concrete. *J. Clean. Prod.* **2022**, *372*, 133649. [CrossRef]
7. Krishna, R.S.; Shaikh, F.; Mishra, J.; Lazorenko, G.; Kasprzhitskii, A. Mine tailings-based geopolymers: Properties, applications and industrial prospects. *Ceram. Int.* **2021**, *47*, 17826–17843. [CrossRef]
8. Capasso, I.; Lirer, S.; Flora, A.; Ferone, C.; Cioffi, R.; Caputo, D.; Liguori, B. Reuse of mining waste as aggregates in fly ash-based geopolymers. *J. Clean. Prod.* **2019**, *220*, 65–73. [CrossRef]
9. Li, F.; Cui, X.; Liu, X.; He, L.; Nan, N.; Zhou, C.; Fan, X. Research on Activation Process of Low Activity Molybdenum Tailings. *Non-Met. Mines* **2021**, *44*, 72–75.
10. Li, F.; Cui, X.; Liu, X.; Tang, Y.; Wang, Z.; Zhou, C.; Fan, X. Research on Preparation of Geochemical Cementitious Materials with Activated Molybdenum Tailings. *Non-Met. Mines* **2021**, *44*, 96–99.
11. Han, Q.H.; Wang, A.; Zhang, J.R. Research on the early fracture behavior of fly ash-based geopolymers modified by molybdenum tailings. *J. Clean. Prod.* **2022**, *365*, 132759. [CrossRef]
12. Wang, A.; Liu, H.Z.; Hao, X.F.; Wang, Y.; Liu, X.Q.; Li, Z. Geopolymer Synthesis Using Garnet Tailings from Molybdenum Mines. *Minerals* **2019**, *9*, 48. [CrossRef]
13. Bai, Y.; Guo, W.; Wang, J.; Xu, Z.; Wang, S.; Zhao, Q.; Zhou, J. Geopolymer bricks prepared by MSWI fly ash and other solid wastes: Moulding pressure and curing method optimisation. *Chemosphere* **2022**, *307*, 135987. [CrossRef] [PubMed]
14. Katpady, D.N.; Takewaka, K.; Yamaguchi, T.; Akira, Y. Performance of slag based Shirasu geopolymer cured under ambient condition. *Constr. Build. Mater.* **2020**, *234*, 117210. [CrossRef]
15. Hadi, M.N.S.; Farhan, N.A.; Sheikh, M.N. Design of geopolymer concrete with GGBFS at ambient curing condition using Taguchi method. *Constr. Build. Mater.* **2017**, *140*, 424–431. [CrossRef]
16. Li, X.Y.; Bai, C.Y.; Qiao, Y.J.; Wang, X.D.; Yang, K.; Colombo, P. Preparation, properties and applications of fly ash-based porous geopolymers: A review. *J. Clean Prod.* **2022**, *359*, 132043. [CrossRef]

17. Poornima, N.; Katyal, D.; Revathi, T.; Sivasakthi, M.; Jeyalakshmi, R. Effect of curing on mechanical strength and microstructure of fly ash blend GGBS geopolymer, Portland cement mortar and its behavior at elevated temperature. In Proceedings of the International E-Conference on Advancements in Materials Science and Technology (ICAM), Electr Network, Chennai, INdia, 23–25 November 2020; pp. 863–870.
18. Zhang, N.; Hedayat, A.; Sosa, H.G.B.; Bernal, R.P.H.; Tupa, N.; Morales, I.Y.; Loza, R.S.C. On the incorporation of class F fly-ash to enhance the geopolymerization effects and splitting tensile strength of the gold mine tailings-based geopolymer. *Constr. Build. Mater.* **2021**, *308*, 125112. [CrossRef]
19. Choi, S.C.; Lee, W.K. Effect of Fe_2O_3 on the Physical Property of Geopolymer Paste. In Proceedings of the 2nd International Conference on Advanced Materials and Information Technology Processing (AMITP 2012), Taipei, Taiwan, 17–18 October 2012; pp. 126–129.
20. Yang, J.; Xu, L.H.; Wu, H.Q.; Jin, J.; Liu, L. Microstructure and mechanical properties of metakaolin-based geopolymer composites containing high volume of spodumene tailings. *Appl. Clay Sci.* **2022**, *218*, 106412. [CrossRef]
21. Tong, G.; Zhang, W.; Gao, Y.; Tang, X. Mechanical Properties and Micromechanism of Alkali-activated Fly Ash Geopolymer. *Mater. Rev.* **2022**, *36*, 20100278-6.
22. Zhu, X.Y.; Lu, C.H.; Li, W.K.; Zhou, S.Q.; Li, F.; Xiao, J.Z.; Shah, S.P. Effects of carbon nanofibers on hydration and geopolymerization of low and high-calcium geopolymers. *Cem. Concr. Compos.* **2022**, *133*, 104695. [CrossRef]
23. Zhang, Z.H.; Li, L.F.; Ma, X.; Wang, H. Compositional, microstructural and mechanical properties of ambient condition cured alkali-activated cement. *Constr. Build. Mater.* **2016**, *113*, 237–245. [CrossRef]
24. Li, N.; Shi, C.J.; Wang, Q.; Zhang, Z.H.; Ou, Z.H. Composition design and performance of alkali-activated cements. *Mater. Struct.* **2017**, *50*, 178. [CrossRef]
25. Leong, H.Y.; Ong, D.E.L.; Sanjayan, J.G.; Nazari, A. Suitability of Sarawak and Gladstone fly ash to produce geopolymers: A physical, chemical, mechanical, mineralogical and microstructural analysis. *Ceram. Int.* **2016**, *42*, 9613–9620. [CrossRef]
26. Tan, J.W.; De Vlieger, J.; Desomer, P.; Cai, J.M.; Li, J.B. Co-disposal of construction and demolition waste (CDW) and municipal solid waste incineration fly ash (MSWI FA) through geopolymer technology. *J. Clean. Prod.* **2022**, *362*, 132502. [CrossRef]
27. Luo, Y.; Klima, K.M.; Brouwers, H.J.H.; Yu, Q.L. Effects of ladle slag on Class F fly ash geopolymer: Reaction mechanism and high temperature behavior. *Cem. Concr. Compos.* **2022**, *129*, 104468. [CrossRef]
28. Mahmoodi, O.; Siad, H.; Lachemi, M.; Dadsetan, S.; Sahmaran, M. Development of normal and very high strength geopolymer binders based on concrete waste at ambient environment. *J. Clean. Prod.* **2021**, *279*, 123436. [CrossRef]
29. Mozgawa, W. The relation between structure and vibrational spectra of natural zeolites. *J. Mol. Struct.* **2001**, *596*, 129–137. [CrossRef]
30. Sarkar, M.; Dana, K. Partial replacement of metakaolin with red ceramic waste in geopolymer. *Ceram. Int.* **2021**, *47*, 3473–3483. [CrossRef]